Progress In Electromagnetics Research M, Vol. 107, 217–229, 2022

In-Situ Measurement Method of Radiation Emission Based on Nonuniform Array and Adaptive Noise Cancelling

Shouyang Zhai[1], Hezhihan Fan[2], Zhongyuan Zhou[2, *], Yan Chen[1], Dan Chen[1], Xiang Zhou[2], and Li Ma[3]

Abstract—For the coexistence of SUT (System Under Test) radiative emission signal and ambient interference signal, the amplitude of SUT signal will be submerged by the amplitude of interference signal, so it is difficult to accurately measure the amplitude of SUT signal. In this paper, a two-level nested array is used as the receiving array antenna, and the mixed matrix estimation method based on Blind Source Separation (BSS) is used to separate the coherent groups of the signal. Then the Sparse Reconstruction method is used for the DOA (Degree Of Arrival) estimation of each coherent group of the signal. After the DOA information of each signal is obtained, beamforming method is used to form beams of the main channel and auxiliary channel. The beam of the main channel outputs without distortion in the direction of the SUT signal and forms zero traps in the direction of the coherent signals, while the beam of the auxiliary channel forms zero traps in both the direction of the SUT signal and the direction of the coherent signal. The data received by the array are respectively multiplied by the weights of the main channel and auxiliary channel to obtain the output signals of the two channels. The output signals of the two channels are respectively fed into the Adaptive Noise Cancellation (ANC) system, and the ANC method is used to suppress the ambient interference signals and restore the SUT signal. Simulation and experiment results show that this method can accurately estimate DOA of radiation emission signals, effectively suppress ambient signals and restore the signal of SUT in field measurement of radiation emission.

1. INTRODUCTION

When measuring radiative emission signals from large equipment systems, we cannot transport them into an anechoic chamber or open field test site, but only in the SUT field. However, the amplitude of the ambient interference present at the test site may exceed the limit of the measurement standard CISPR 16-2-5 [1], which states that the ambient interference is at least 6 dB lower than the radiative emission from the SUT. If the amplitude of these ambient interference signals is too high, we cannot accurately measure the radiative emission signal of SUT.

Svacina et al. proposed a difference method to suppress ambient interference [2]. The premise of this method is that the power spectrum of ambient interference should be nearly the same when SUT is turned off and switched on. Marino and Watkins proposed the virtual anechoic chamber technology based on the principle of Adaptive Noise Cancellation on the premise that no signal related to SUT signal could exist in the ambient interference [3, 4]. The ambient interference suppression method based on array antenna [5, 6] proposed by Lu et al. firstly estimates the degree of arrival (DOA) of all signals through array signal processing technology. Then, the array beam is formed by the beamforming

Received 23 October 2021, Accepted 17 January 2022, Scheduled 27 January 2022
* Corresponding author: Zhongyuan Zhou (zyzhou@seu.edu.cn).
[1] State Key Laboratory of Nuclear Power Safety Monitoring Technology and Equipment, Guangzhou, China. [2] Research Center for Electromagnetic Environment Effects, Southeast University, Nanjing, China. [3] State Key Laboratory of Millimeter Waves, Southeast University, Nanjing, China.

algorithm. The beam has no distortion in the direction of SUT, but forms a "zero trap" in the direction of incoming ambient interference, so as to suppress the ambient interference and restore the SUT radiation signal. However, if the number of ambient interferences is large, it is impossible to form a beam with "zero traps" equal to the number of ambient interferences. Li et al. improved this method. They proposed a coherent group classification method based on a uniform array, which used fewer array elements to solve the problem of multiple signal sources [7, 8]. However, using a uniform array may lead to the coupling between array elements and edge effect [19]. In addition, when a uniform array with fewer elements is used, the resolution of the array beam will be lower due to the smaller array aperture. If a nonuniform array is used, in the case of the same number of array elements, the aperture will become larger, and the resolution of the array will also become higher. Therefore, this article makes improvements on the basis of Li et al.'s research, adopting a two-level nested array structure in a nonuniform array and optimizes the related algorithm proposed by them to make it suitable for a two-level nested array structure. The purpose of DOA estimation and ambient interference suppression with a nonuniform array is realized.

In this paper, based on the nested array, the array signal processing technology is combined with

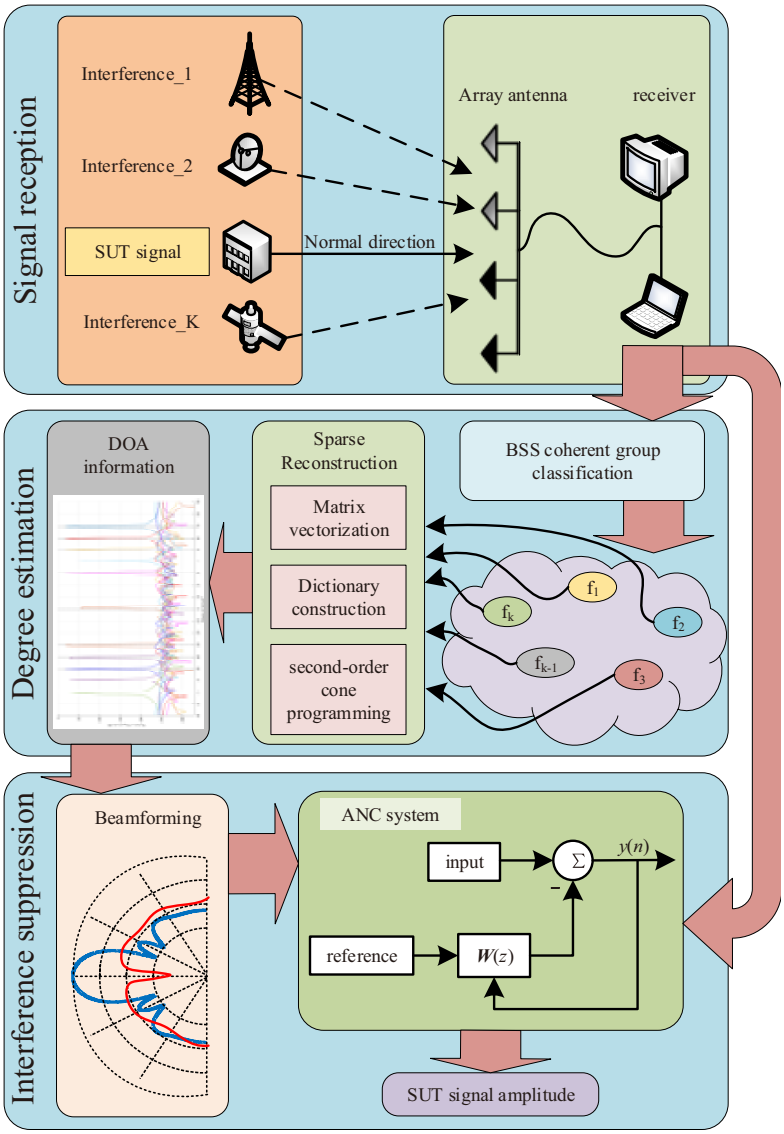

Figure 1. The flow chart of the method presented in this paper.

the ANC technology to realize the suppression of ambient interferences and restore the SUT radiation signals. Firstly, the algorithm of BSS and Sparse Reconstruction is improved to be suitable for a two-level nested array to improve the accuracy of signal DOA estimation. In addition, the signals received by the array are passed into the main channel and auxiliary channel, respectively. Beam traps are generated in the main channel to suppress the coherent signals, but the SUT signal is outputted without distortion. The auxiliary channel is filtered by Spatial Matrix Filtering to suppress both SUT radiation signal and coherent signal. Finally, the correlation of other signals is used to connect the signals of two channels into an ANC system to achieve the restoration of SUT signal. For the above content, please refer to the flowchart in Fig. 1.

2. BASIC PRINCIPLES AND ALGORITHMS

2.1. Array and Received Signal Models

Pal and Vaidyanathan proposed a kind of classical nonuniform array, that is, nested array [9]. This article mainly introduces a two-level nested array, so the nested array referred to in the following paragraphs is a two-level nested array unless otherwise specified.

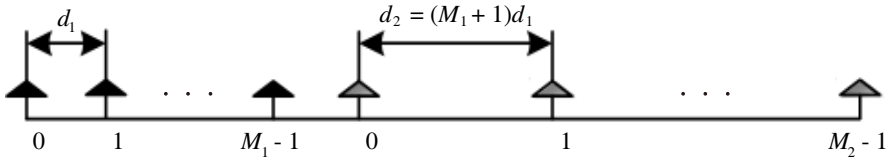

Figure 2. A two-level nested array.

As shown in Fig. 2, the nested array consists of two subarrays with a total of M elements ($M = M_1 + M_2$). Subarray 1 is a dense uniform array with array element number M_1 and array element spacing $d_1 = \lambda/2$. Subarray 2 is a sparse uniform array, with array element number M_2 and array element spacing $d_2 = (M_1 + 1)d_1$. λ stands for the incident signal wavelength. The array element positions of nested arrays are expressed as:

$$\mathrm{S}_{NA} = \{s_1, s_2, \cdots, s_M\} = \{0, 1, \cdots, M_2(M_1 + 1) - 1\} \tag{1}$$

Through the array element position set S_{NA}, the position difference set $\mathrm{F}_{NA} = \{s_i - s_j \,|s_i, s_j \in \mathrm{S}_{NA}\}$ of the array element can be obtained. Removing redundant elements from F_{NA}, we get the contiguous set $\bar{\mathrm{F}}_{NA} = \left\{-\bar{M} + 1, \cdots, -1, 0, 1, \cdots, \bar{M} - 1 \,\middle|\, \bar{M} = M_2(M_1 + 1)\right\}$.

Assuming that there are K independent signals incident into the nested array, the mathematical model of the received signal is expressed as:

$$\mathbf{X}(t) = \mathbf{A}(\theta)\mathbf{s}(t) + \mathbf{n}(t) \tag{2}$$

where $\mathbf{X}(t)$ is the received signal of the array, $\mathbf{A}(\theta)$ the array manifold matrix, $\mathbf{s}(t)$ the signal source vector, and $\mathbf{n}(t)$ the noise vector.

After the received signal of the array is obtained, its covariance matrix $\mathbf{R}_{XX}$ is calculated, and then $\mathbf{z}$ is obtained after vectorization. σ_k^2 and σ_n^2 denote the power of the incident signal and noise, respectively [9].

$$\mathbf{R}_{XX} = E\left\{\mathbf{X}(t)\mathbf{X}^H(t)\right\} = \sum_{k=1}^{K} \sigma_k^2 a(\theta_k) a^H(\theta_k) + \sigma_n^2 \mathbf{I}_M \tag{3}$$

$$\mathbf{z} = \mathrm{vec}(\mathbf{R}_{XX}) = \mathbf{B}\mathbf{p} + \sigma_n^2 \mathbf{e} \tag{4}$$

where $\mathrm{vec}(\cdot)$ represents the vectorization operation, and $\mathbf{p}$ represents the signal power vector, $\mathbf{p} = \left[\begin{array}{cccc} \sigma_1^2 & \sigma_2^2 & \cdots & \sigma_K^2 \end{array}\right]^T$. Besides, $\mathbf{e} = \left[\begin{array}{cccc} \mathbf{e}_1^T & \mathbf{e}_2^T & \cdots & \mathbf{e}_M^T \end{array}\right]$, with $\mathbf{e}$ being the column vector of all zeros except the 1 at the i-th position.

$$\mathbf{B} = \left[\begin{array}{cccc} \mathbf{b}(\theta_1) & \mathbf{b}(\theta_2) & \cdots & \mathbf{b}(\theta_K) \end{array}\right],$$

$$\mathbf{b}(\theta_K) = a^*(\theta_k) \otimes a(\theta_k) = \left[\begin{array}{cccc} \eta_1^T(\theta_k) & \eta_2^T(\theta_k) & \cdots & \eta_M^T(\theta_k) \end{array} \right]^T \in \mathbb{C}^{M^2 \times 1},$$

$\otimes$ represents the Kronecker product operation, and $(\cdot)^*$ is the conjugate.

$$\eta_i(\theta_k) = \left[\begin{array}{cccc} e^{-j\frac{2\pi}{\lambda}(s_1 - s_i)d\sin\theta_k} & e^{-j\frac{2\pi}{\lambda}(s_2 - s_i)d\sin\theta_k} & \cdots & e^{-j\frac{2\pi}{\lambda}(s_M - s_i)d\sin\theta_k} \end{array} \right] \in \mathbb{C}^{M \times 1} \tag{5}$$

By comparative analysis of Eqs. (4) and (2), it is found that the two formulae have similar mathematical expressions. Eq. (4) can be regarded as the receiving signal of a virtual array, and the element position of the virtual array corresponds to the array element position difference set F_{NA} of the nonuniform array. Of course, there are repeated elements in both the vector $\mathbf{z}$ and the set F_{NA}. By de-redundancy and rearrangement of $\mathbf{z}$, a new vector $\mathbf{z}_1$ can be obtained, in which the elements correspond to $\bar{\mathrm{F}}_{NA}$.

2.2. Coherent Group Classification Based on BSS

In this method, the mixed matrix is estimated based on the sparsity of signals in time-frequency domain. Since most signals do not meet the condition of separable sparsity in time domain, Short-Time Fourier Transform (STFT) is used in this paper to perform sparse representation of signals [10].

The STFT of Eq. (2) can be obtained as $\mathbf{X}(t, f)$:

$$\mathbf{X}(t, f) = \mathbf{A}\mathbf{S}(t, f) + \mathbf{n}(t, f), \quad (t, f) \in \Omega \tag{6}$$

Ω represents the entire time-frequency plane, and time-frequency support points are screened from all time-frequency points according to the following equation:

$$\|\mathbf{X}(t, f)\|_2^2 > \xi \tag{7}$$

Let the number of time-frequency points satisfying Equation (7) be P, and ξ be the threshold value related to noise.

Calculate the time-frequency ratio between each array element observation signal and the m-th array element observation signal. In this paper, take $m = 1$, and the time-frequency ratio matrix can be obtained:

$$D = \left[\begin{array}{cccc} \dfrac{X_1(t_1, f_1)}{X_1(t_1, f_1)} & \dfrac{X_1(t_2, f_2)}{X_1(t_2, f_2)} & \cdots & \dfrac{X_1(t_P, f_P)}{X_1(t_P, f_P)} \\ \dfrac{X_2(t_1, f_1)}{X_1(t_1, f_1)} & \dfrac{X_2(t_2, f_2)}{X_1(t_2, f_2)} & \cdots & \dfrac{X_2(t_P, f_P)}{X_1(t_P, f_P)} \\ \vdots & \vdots & \ddots & \vdots \\ \dfrac{X_M(t_1, f_1)}{X_1(t_1, f_1)} & \dfrac{X_M(t_2, f_2)}{X_1(t_2, f_2)} & \cdots & \dfrac{X_M(t_P, f_P)}{X_1(t_P, f_P)} \end{array} \right] \in \mathbb{C}^{M \times P} \tag{8}$$

The second line in Eq. (8) is taken as the research object:

$$D_2 = \left[\begin{array}{cccc} \dfrac{X_2(t_1, f_1)}{X_1(t_1, f_1)} & \dfrac{X_2(t_2, f_2)}{X_1(t_2, f_2)} & \cdots & \dfrac{X_2(t_P, f_P)}{X_1(t_P, f_P)} \end{array} \right] \tag{9}$$

It is considered that the time-frequency ratio of single source points (SSPs) belonging to the same coherent group is a complex constant. Due to the influence of noise, the time-frequency ratio will not be a constant, but will be gathered in a subinterval. All time-frequency ratios in D_2 are counted, and their real and imaginary parts are taken. The whole complex field formed by the real and imaginary parts is divided into several subintervals so that the SSPs belonging to a coherent group can fall into the same subinterval as much as possible.

2.3. DOA Estimation Based on Sparse Reconstruction

After coherent group classification, the corresponding time-frequency support point matrix can be found through the SSPs in each coherent group. Suppose that there are Q coherent groups, and the time-

frequency support point matrix corresponding to each coherent group is:

$$\mathbf{X}(t,f)_i = \begin{bmatrix} X_1(t_1,f_1) & X_1(t_2,f_2) & \cdots & X_1(t_{L_i},f_{L_i}) \\ X_2(t_1,f_1) & X_2(t_2,f_2) & \cdots & X_2(t_{L_i},f_{L_i}) \\ \vdots & \vdots & \ddots & \vdots \\ X_M(t_1,f_1) & X_M(t_2,f_2) & \cdots & X_M(t_{L_i},f_{L_i}) \end{bmatrix} \tag{10}$$

Among them, $L_i\,(i=1,2,...,Q)$ is the number of SSPs in each coherent group, $\sum_{i=1}^{Q} L_i = P$, and P is the number of all time-frequency support points satisfying Eq. (7).

For $\mathbf{X}(t,f)_i$, the covariance matrix is first solved, then the vectorization operation is carried out, and the redundant elements are removed to obtain a one-dimensional column vector $\mathbf{z}_{1i}\,(i=1,2,...,Q)$.

The elements in $\mathbf{z}_{1i}$ correspond to the virtual continuous array elements of the nested array, that is, to the set $\bar{\mathrm{F}}_{NA}$. Since the influence of noise has been ignored in the time-frequency support point, so:

$$\mathbf{z}_{1i} = \mathbf{B}_i \mathbf{p}_i \tag{11}$$

Since the signal distribution in each coherent group is sparse in spatial domain, the estimation of the DOA can be regarded as a problem of sparse vector reconstruction. The values of the non-zero elements in the sparse vector and their positions in the vector respectively represent the amplitude and degree of the incident signal.

Based on the Compressed Sensing theory, the array guide vector matrix $\mathbf{B}_i$ can be extended into an over-complete dictionary. Let $\{\ \tilde{\theta}_1 \quad \tilde{\theta}_2 \quad \cdots \quad \tilde{\theta}_N\ \}$ represent the set of all possible directions, and $\{\ \theta_1 \quad \theta_2 \quad \cdots \quad \theta_K\ \}$ represent the actual direction of arrival, and $N \gg K$.

Constructing an over-complete dictionary:

$$\mathbf{B}_D = \left[\ b(\tilde{\theta}_1) \quad b(\tilde{\theta}_2) \quad \cdots \quad b(\tilde{\theta}_N)\ \right] \tag{12}$$

We need to find a sparse $\mathbf{h} = [\ h_1 \quad h_2 \quad \cdots \quad h_N\ ]^T \in \mathbb{C}^{N\times 1}$ so that:

$$\min_{\mathbf{h}} \|\mathbf{z}_{1i} - \mathbf{B}_D\mathbf{h}\|_2^2 + \eta \|\mathbf{h}\|_1 \tag{13}$$

The parameter η controls the balance between sparsity and residual norm, and the angle $\tilde{\theta}_i$ of $\mathbf{h}$ non-zero elements represents the DOAs of signals in the coherent group. In order to optimize Eq. (13), we adopt the second-order cone programming method [11, 12] and convert it into:

$$\begin{aligned} &\min \quad s + \eta q \\ &\text{s.t.} \quad \|\mathbf{Z}\|_2^2 \le s, \ \text{ and } \ \mathbf{lt} \le q \\ &\text{where} \quad \sqrt{\sum_{i=1}^{N} h_i^2} \le t_i, \ \text{ for } \ i = 1,2,...,N \\ &\text{and} \quad \mathbf{Z} = \mathbf{z}_{1i} - \mathbf{B}_D\mathbf{h} \end{aligned} \tag{14}$$

In the formula, $\mathbf{l}$ is a 1 by N dimension 1 vector.

2.4. Beamforming and Adaptive Noise Cancellation

After obtaining the DOA of the signals, we need to realize the design of the main channel beam and the auxiliary channel beam. The optimization of the main channel beam in this section can be described as:

$$\begin{aligned} &\min_{w_1} \ \max \|p(\Theta_0) - 0\,(\mathrm{dB})\|_2 \\ &\text{s.t.} \ \ \|p(\Theta_{\mathrm{NULL}})\|_2 \le -50 \end{aligned} \tag{15}$$

In the formula, Θ_0 represents the incident orientation of SUT signal. Since the incident direction of the SUT signal in this paper is the normal direction of the array, the incident angle of the SUT signal

is 0°. Θ_{NULL} represents the incident orientation of coherent signal, and Θ_{NULL} is derived from the DOA estimation method proposed in Section 2.2 and Section 2.3. $p(\Theta_0)$ and $p(\Theta_{\mathrm{NULL}})$ represent the normalized amplitude. Under the premise of ensuring the zero trap of the incident degree azimuth beam of the coherent signal at -50 dB, the SUT radiation signal is kept from distortion as far as possible. In this paper, particle swarm beam optimization method [13–15] is used to form the main channel beam.

Beam optimization of the auxiliary channel can be described as:

$$\begin{aligned} &\min_{w_2} \ \max p(\Theta_S) \\ &\text{s.t.} \ \ -20 \le \|p(\Theta_{SL})\|_2 \le -10 \end{aligned} \tag{16}$$

where Θ_S represents the incident orientation of SUT and coherent signals; Θ_{SL} represents the angle range of beam sidelobe; $p(\Theta_S)$ and $p(\Theta_{SL})$ represent the normalized amplitude. Under the premise that the sidelobes level is in the range of -20 dB ~ -10 dB, the SUT radiation signal and coherent signal are minimized. In this paper, the method of Spatial Matrix Filtering [16–18] is used to form the auxiliary channel beam.

The main channel signal is used as the original input signal, and the auxiliary channel signal is used as the reference input signal. The ANC system is shown in Fig. 3. The weight vector of the adaptive filter is adjusted to minimize the mean square error between the output signal of the ANC system and the useful signal, and the resulting output signal is the restored SUT signal [8].

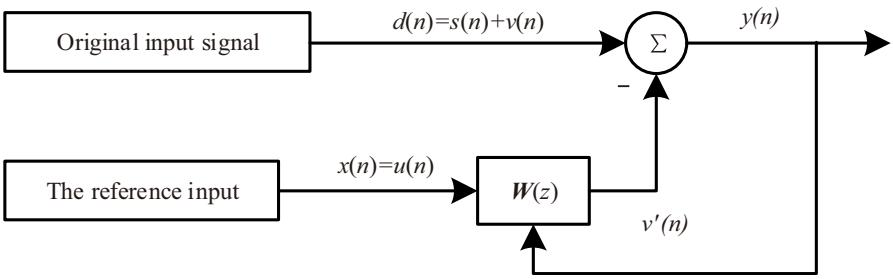

Figure 3. Adaptive Noise Cancellation (ANC) system.

In Fig. 3, $d(n)$ is the original input, $x(n)$ the reference input, $s(n)$ the useful signal, $v(n)$ the noise, and $u(n)$ is unrelated to $s(n)$ and $v(n)$. The $v'(n)$ obtained by multiplying $u(n)$ by the adaptive filter weights $\mathbf{W}(z)$ is unrelated to $s(n)$, so the output of the ANC system is:

$$y(n) = s(n) + v(n) - v'(n) \tag{17}$$

Take the square of both sides:

$$y^2(n) = s^2(n) + (v(n) - v'(n))^2 + 2s(n)(v(n) - v'(n)) \tag{18}$$

Take mean of both sides of Eq. (18), since $s(n)$ and $v(n)$ are independent of $v'(n)$, so:

$$E[y^2(n)] = E\left[s^2(n)\right] + E[(v(n) - v'(n))^2] \tag{19}$$

Therefore, adjusting the filter weights to minimize $E[y^2(n)]$ is equivalent to minimize $E[(v(n) - v'(n))^2]$, and when $E[(v(n) - v'(n))^2]$ is the smallest, it is equivalent to $E[(y(n) - s(n))^2]$ smallest, that is, the mean square error between the output signal $y(n)$ and the useful signal $s(n)$ is the smallest. In other words, $y(n)$ is the minimum estimate of the mean square error of the useful signal $s(n)$ extracted from the original input signal $d(n)$.

3. SIMULATION AND ANALYSIS

In this section, the method proposed in the previous section is simulated and analyzed. The number of nested array elements used is 6; subarray 1 is 3; and subarray 2 is 3. The mathematical form of each

incident signal is as follows:

$$\begin{cases} s_{\mathrm{SUT}}(t) = 10 * \exp(j2\pi f_0 t) \\ s_1(t) = 100 * \exp(j2\pi f_0 t + \pi/3) \\ s_2(t) = 100 * \exp(j2\pi f_1 t) \\ s_3(t) = 100 * \exp(j2\pi f_2 t) \\ s_4(t) = 100 * \exp(j2\pi f_3 t) \\ s_5(t) = 100 * \exp(j2\pi f_4 t + \pi/2) \\ s_6(t) = 80 * \exp(j2\pi f_4 t) \\ s_7(t) = 100 * \exp(j2\pi f_5 t) \\ s_8(t) = 100 * \exp(j2\pi f_6 t) \\ s_9(t) = 100 * \exp(j2\pi f_7 t) \\ s_{10}(t) = 100 * \exp(j2\pi f_8 t) \end{cases} \tag{20}$$

The incident angle of SUT signal is 0°, and the incident angles of other ambient signals are −30°, −70°, 70°, 60°, −40°, −60°, 40°, 50°, −50°, 30° in turn. The frequency of $s_{\mathrm{SUT}}(t)$ and $s_1(t)$ is $f_0 = 933\,\mathrm{MHz}$, and the frequencies of other ambient signals are $f_1 = 910\,\mathrm{MHz}$, $f_2 = 920\,\mathrm{MHz}$, $f_3 = 940\,\mathrm{MHz}$, $f_4 = 950\,\mathrm{MHz}$, $f_5 = 960\,\mathrm{MHz}$, $f_6 = 970\,\mathrm{MHz}$, $f_7 = 980\,\mathrm{MHz}$, $f_8 = 990\,\mathrm{MHz}$. The amplitude of each signal is in mV.

As shown in Fig. 4, Fig. 4(a) shows the signal spectrum without processing; Fig. 4(b) and Fig. 4(c) show the scatter distribution in the second row of the time-frequency ratio matrix; Fig. 4(b) shows the scatter plots without screening; and Fig. 4(c) shows the scatter plots after preliminary screening.

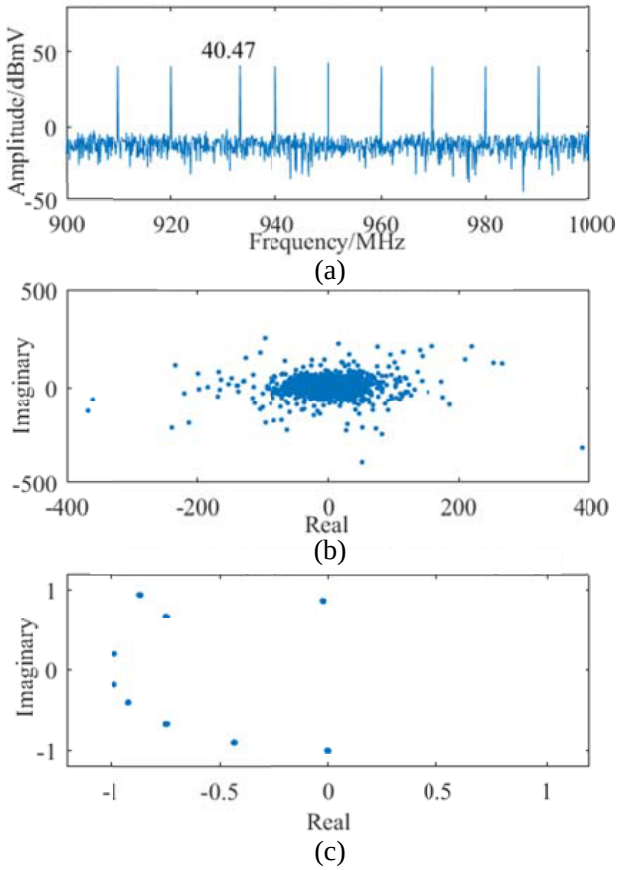

Figure 4. Signal spectrum diagram and time-frequency scatter points. (a) Diagram of the SUT signal and the interference. (b) Time-frequency support points. (c) SSPs belonging to different coherent groups.

The scatter points in Fig. 4(c) are meshed so that the scatter points in each subinterval are aggregated as much as possible. As shown in Fig. 4(c), we separated 9 coherent groups and performed DOA estimation on each coherent group to obtain the following results.

In Fig. 5, each color represents a coherent group. It can be seen that $s_{\mathrm{SUT}}(t)$ is coherent with $s_1(t)$; $s_5(t)$ is coherent with $s_6(t)$; and other signals are unrelated. The error of DOA estimation results is within 2°. However, if the uniform array of 6 elements and the method in [7] are used to estimate the arrival angle, the result will not be so ideal. As shown in Fig. 6, many angles have not been estimated.

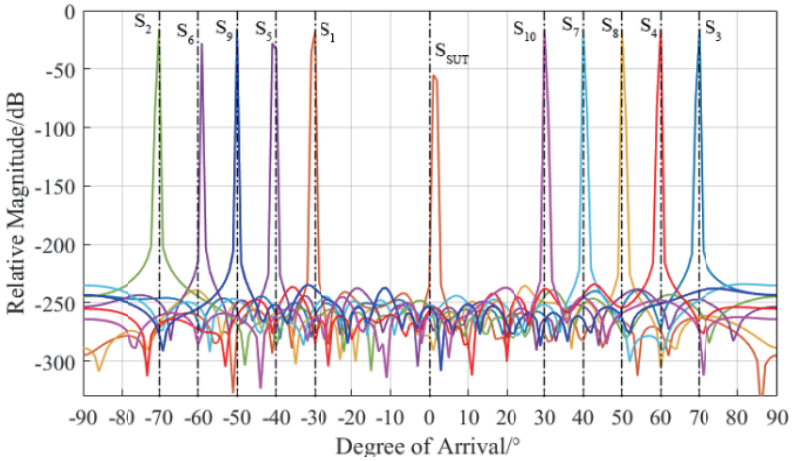

Figure 5. DOAs estimated by non-uniformed array.

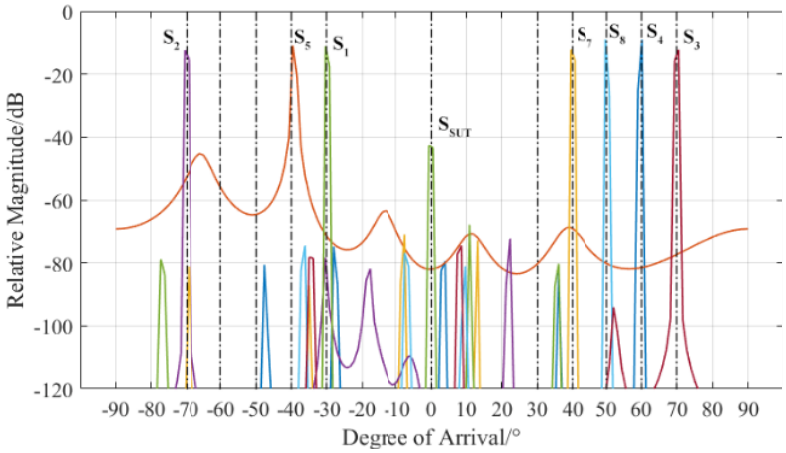

Figure 6. DOAs estimated by uniformed array.

Based on the measured DOA of the SUT signal and coherent signal, the main channel and auxiliary channel beams are generated by the Particle Swarm Optimization algorithm and the Spatial Matrix Filtering, Fig. 7. The generated main channel beam forms a zero trap of more than -50 dB in the incident angle of coherent signal $s_1(t)$, while there is no attenuation in the direction of SUT signal. The auxiliary channel beam forms two traps of more than -50 dB on the incident angles of both coherent signals $s_1(t)$ and $s_{\mathrm{SUT}}(t)$.

The signals of the two channels are input into the ANC system to restore the SUT signal.

In Fig. 8, Fig. 8(a) is the output signal of the main channel; Fig. 8(b) is the output signal of the auxiliary channel; and Fig. 8(c) is the SUT signal restored by the ANC method. Its amplitude is 20 dBmV, which is consistent with the preset conditions, and the environmental signal is suppressed by more than 40 dB.

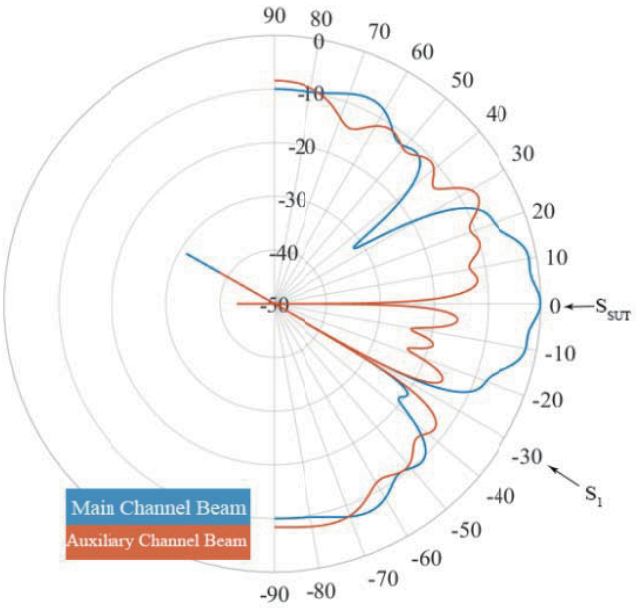

Figure 7. Beam pattern of main channel and auxiliary channel.

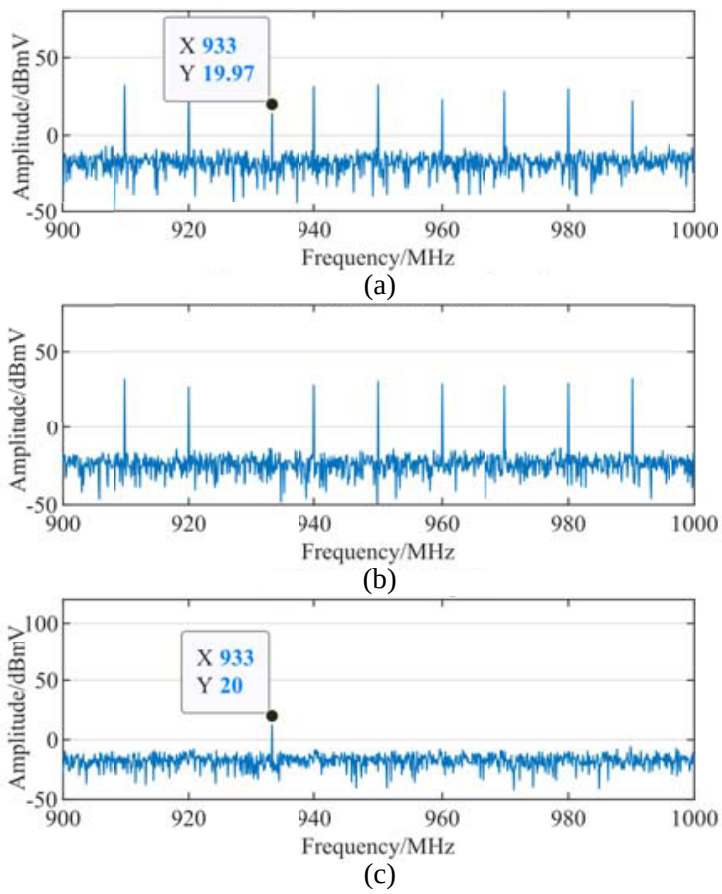

Figure 8. Main channel and auxiliary channel output signal and the restored signal.

4. TEST EXPERIMENT AND ANALYSIS

The experiment designed in this section uses four small microstrip patch antennas as array elements to form a nonuniform array (the number of elements in subarray 1 is 1, and the number of elements in subarray 2 is 3), to measure the mixed signal when the SUT signal and ambient signal coexist. Then the approach proposed in this paper is used to estimate the DOA of the signal and restore the signal of SUT.

As shown in Fig. 9, the signal source of SUT is set in the normal direction of the array, and the ambient signal source is set in the 45° direction of the array. The distance between the transmitting antenna and receiving array antenna is greater than 5.3 m, that is, more than ten times the aperture of the array, and it can be considered as a far-field source. Fig. 10 shows the actual measurement arrangement in the anechoic room, and Table 1 is the model of each instrument.

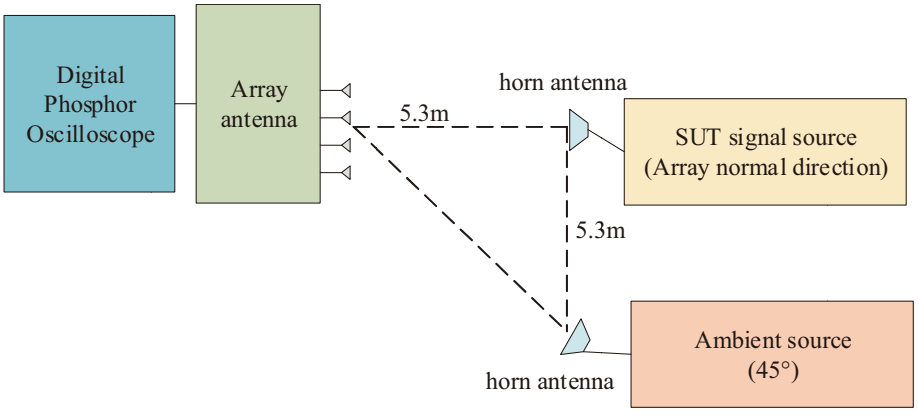

Figure 9. Schematic diagram of experiment.

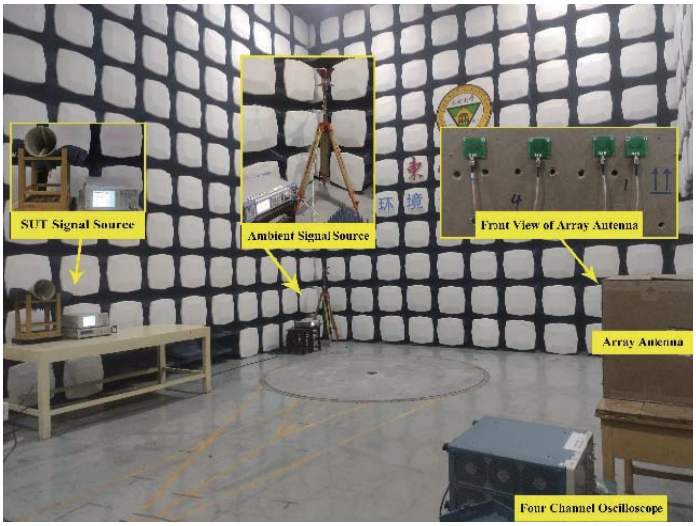

Figure 10. The experimental arrangement.

The experiment is divided into two groups. The first group simulates the existence of coherent signals, and the second group simulates the existence of incoherent signals. The first group sets the frequency of SUT signal at 2.9 GHz and the frequency of ambient signal at 2.9 GHz. The second test sets the frequency of SUT signal at 2.9 GHz and the frequency of ambient signal at 3 GHz. The data processing results are shown in Fig. 11.

Table 1. Instrument list.

Signal generators	Keysight N9310A; Rohde & Schwarz SMB 100A
Transmitting antennas	High frequency horn antennas
Receiving antenna	Array antenna
Oscilloscope	Tektronix DPO 71604C

In Fig. 11, Fig. 11(g) is the signal amplitude measured when only the SUT signal source is turned on, which is −58.35 dBmV. Fig. 11(a) is the DOA estimated by the first group of experiments; the SUT incident angle is −5°; and the coherent signal incident angle is 44°. Fig. 11(c) shows the amplitude of the mixed signal received by the array in the first group of experiments, which is −46.95 dBmV. Fig. 11(e) shows the restored SUT signal with an amplitude of −61.78 dBmV. In the first group, we

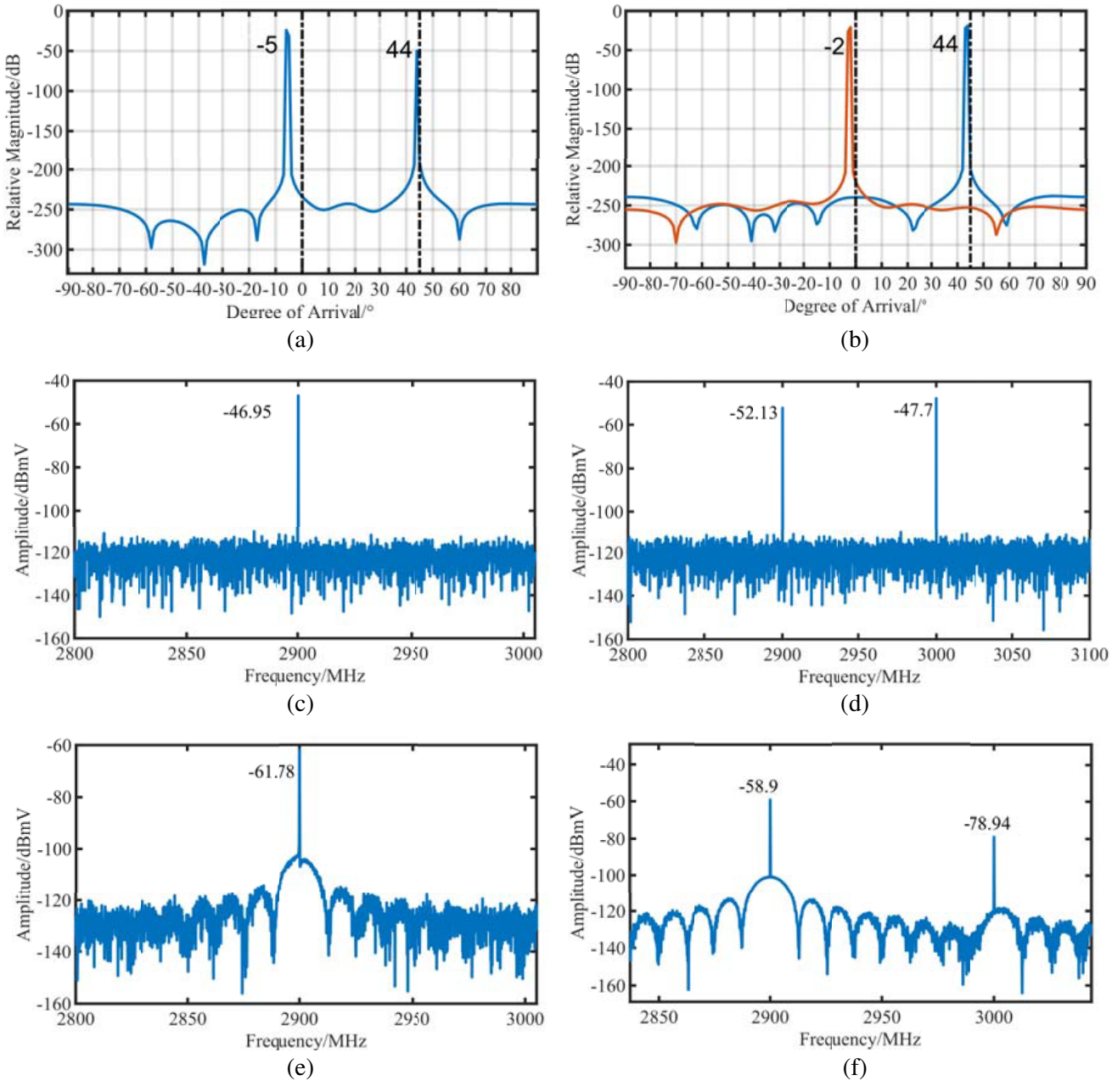

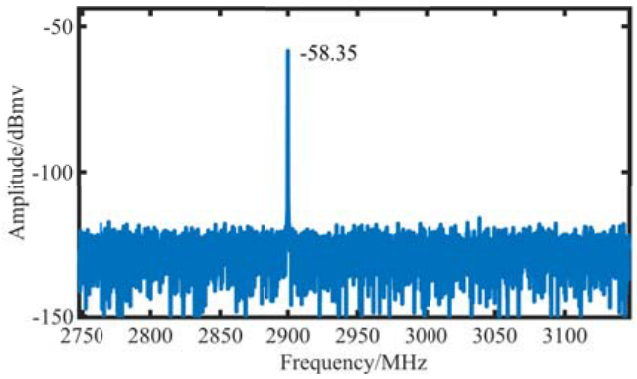

(g)

Figure 11. The experimental result. (a) DOA estimation when coherent signal exists. (b) DOA estimation when incoherent signal exists. (c) Measurement of SUT signal and coherent signal. (d) Measurement of SUT signal and incoherent signal. (e) The restored SUT signal. (f) The restored SUT signal. (g) SUT signal measurement value.

suppressed the interference of the mixed signal with an amplitude of −46.95 dBmV, and finally restored it to −61.78 dBmV, and the error between the real signal amplitude −58.35 dBmV was 3.43 dB.

Figure 11(b) is the DOAs estimated by the second group of experiments; the SUT incident angle is −2°; and the incoherent signal incident angle is 44°. Fig. 11(d) shows the mixed signals received by the array in the second group of experiments, with an amplitude of −52.13 dBmV at 2.9 GHz and −47.7 dBmV at 3 GHz. Fig. 11(f) shows the restored SUT signal. The amplitude of 2.9 GHz is −58.9 dBmV, and that of 3 GHz is −78.94 dBmV, indicating that the ambient signal is greatly suppressed. In the second group of experiments, the error between the restored 2.9 GHz SUT signal amplitude and the real SUT signal amplitude is 0.55 dB.

Although the amplitude of the ambient interference signal in Fig. 11(f) still exists, it has been suppressed by about 30 dB compared with the amplitude in Fig. 11(d), which can be clearly distinguished from the amplitude of the SUT signal. The suppression range of ambient interference is related to the beam "zero trap" designed in this experiment, which is basically in line with the design.

5. CONCLUSION

In this paper, a two-level nested array is used as the receiving array antenna to study the in-situ measurement method. The received signals of the array are processed by BSS and Sparse Reconstruction algorithm to estimate the degree of arrival of each signal. Based on the measured DOA, the ambient signal was suppressed by combining the method of beamforming and ANC, and the amplitude of SUT signal was finally restored.

Since the ideal distance between the elements of the sub-array 1 is half the wavelength of the incident signal, the size of the array in this article has a great correlation with the frequency of the incident signal. If the frequency range is too large, the DOA estimated by this method may be inaccurate, so the frequency range studied in this paper is about 100 MHz: the frequency range of simulation is 900 MHz–1 GHz, and the frequency range of experiment is 2.9 GHz–3 GHz.

In the simulation, we used a nested array of six elements to estimate the DOA of 11 signals, suppressed the amplitude of the environmental interference signal by more than 40 dB, and finally recovered the signal amplitude of the SUT. In the experiment, we used a nested array of 4 elements to test the coherent interference signal and the uncorrelated interference signal, respectively. When the coherent interference signal exists, the DOA estimation error of the SUT reaches 5°, and the SUT amplitude recovery error is 3.43 dB. When the uncorrelated interference signal exists, the DOA estimation error of the SUT is 2°, and the SUT amplitude restoration error is 0.55 dB.

REFERENCES

1. Specification for radio disturbance and immunity measuring apparatus and methods — Part 2–5: In situ measurements of disturbing emissions produced by physically large equipment, CISPR 16-2-5, 2008.
2. Svacina, J., J. Drinovsky, and R. Videnka, "Virtual anechoic room an useful tool for EMI pre-compliance testing," *2007 17th International Conference Radioelektronika*, 1–4, Brno, Czech Republic, 2007.
3. Marino, M. and S. D. Watkins, "EMI ambient cancellation and source localization technology," *1999 International Symposium on Electromagnetic Compatibility (IEEE Cat. No. 99EX147)*, 807, Tokyo, Japan, 1999.
4. Marino, M. A., "System and method for measuring RF radiated emissions in the presence of strong ambient signals," U.S. Patent 698 0611 B1, 2005.
5. Lu, Z., J. Liu, and P. Liu, "A novel method of ambient interferences suppressing for in situ electromagnetic radiated emission test," *IEEE Transactions on Electromagnetic Compatibility*, Vol. 54, No. 6, 1205–1215, Dec. 2012.
6. Lu, Z., L. Ding, X. Lin, and M. Lin, "An innovative virtual chamber measurement method based on spatial domain cancellation technique for radiation emission in situ test," *IEEE Transactions on Electromagnetic Compatibility*, Vol. 59, No. 2, 342–351, Apr. 2017.
7. Zhou, Z., P. Li, M. Sheng, Q. Zhou, and P. Hu, "Ambient interferences suppressing for in-situ radiated emissions measurement based on array signal processing and adaptive noise cancellation," *IEEE Transactions on Electromagnetic Compatibility*, Vol. 62, No. 4, 1055–1067, Aug. 2020.
8. Li, P., Z. Y. Zhou, M. J. Sheng, Q. Zhou, and P. Hu, "In situ measurement of radiated emissions based on array signal processing and adaptive noise cancellation," *IEICE Trans. Electron.*, Vol. E102-C, No. 4, 371–379, 2019.
9. Pal, P. and P. P. Vaidyanathan, "Nested arrays: A novel approach to array processing with enhanced degrees of freedom," *IEEE Trans. on Signal Processing*, Vol. 58, No. 8, 4167–4181, 2010.
10. Li, Y. Q., A. Cichocki, and S. I. Amari, "Analysis of sparse representation and blind source separation," *Neural Computation*, Vol. 16, No. 6, 1193–1234, 2004.
11. Malioutov, D., M. Cetin, and A. S. Willsky, "A sparse signal reconstruction perspective for source localization with sensor arrays," *IEEE Transactions on Signal Processing*, Vol. 53, No. 8, 3010–3022, Aug. 2005.
12. Tian, Y. and X. Y. Sun, "Passive localization of mixed sources jointly using MUSIC and sparse signal reconstruction," *AEU — International Journal of Electronics and Communications*, Vol. 68, No. 6, 534–539, 2014.
13. Kennedy, J. and R. Eberhart, "Particle swarm optimization," *Proceedings of ICNN'95 — International Conference on Neural Networks*, Vol. 4, 1942–1948, Perth, WA, Australia, 1995.
14. Robinson, J. and Y. Rahmat-Samii, "Particle swarm optimization in electromagnetics," *IEEE Transactions on Antennas and Propagation*, Vol. 52, No. 2, 397–407, Feb. 2004.
15. Cao, D., A. Modiri, G. Sureka, and K. Kiasaleh, "DSP implementation of the particle swarm and genetic algorithms for real-time design of thinned array antennas," *IEEE Antennas and Wireless Propagation Letters*, Vol. 11, 1170–1173, 2012.
16. Van Veen, B. D. and K. M. Buckley, "Beamforming: A versatile approach to spatial filtering," *IEEE ASSP Magazine*, Vol. 5, No. 2, 4–24, Apr. 1988.
17. Hassanien, A. and S. A. Vorobyov, "A robust adaptive dimension reduction technique with application to array processing," *IEEE Signal Processing Letters*, Vol. 16, No. 1, 22–25, Jan. 2009.
18. Hassanien, A., S. A. Elkader, A. B. Gershman, and K. M. Wong, "Convex optimization based beamspace preprocessing with improved robustness against out-of-sector sources," *IEEE Transactions on Signal Processing*, Vol. 54, No. 5, 1587–1595, May 2006.
19. Ge, X., Z. Zhou, and Y. Gu, "Improvement on in-situ radiated emission measurement method," *2021 IEEE 5th Advanced Information Technology, Electronic and Automation Control Conference (IAEAC)*, 1080–1084, 2021.